INTERNATIONAL JOURNAL
FOR RESEARCH

IN APPLIED SCIENCE & ENGINEERING TECHNOLOGY

Analysis of a Grid-Tie Solar Power System for Efficient Transition between Grid-Connected Modes

Mamta[1], Dr. M.K. Bhaskar[2], Manish Parihar[3]
Electrical Engg. Department, M.B.M. University, Jodhpur (Raj)

Abstract: Solar Photo Voltaic (PV)-battery energy storage based micro-grid with a multifunctional Voltage Source Converter (VSC) is presented in this research paper. Whenever the grid fails, this system operates in SA mode automatically, thereby without causing any interruption in supplying the load. Similarly, it automatically shifts to the GC mode, when the grid is restored. The VSC functions in current control for GC mode, and it operates in voltage control for SA mode of operation. This system is capable of extracting the maximum power from the solar PV array irrespective it is operating in the GC mode or SA mode. It regulates the dc-link voltage to the maximum power point voltage of the PV array. If the absence of the battery is detected, then the control is automatically shifted to VSC for performing the extraction of the maximum power of the PV array.
Keywords: Battery energy storage (BES), bidirectional dc–dc converter (BDDC), grid connected (GC) mode, power quality, solar photovoltaic (PV) array, standalone (SA) mode.

I. INTRODUCTION

Depletion of conventional energy sources and environmental impacts, the role of renewable sources for energy generation has become a prior choice nowadays. Due to the ease of availability, environment friendly nature, and the reducing trends in the cost of solar photovoltaic (PV) panels, solar-based energy generation has become popular as compared to other energy sources [1]. The main drawback of solar energy is its intermittent nature. So the PV array alone is not possible to meet the load demand at every time. This causes poor reliability of the system. This problem is overcome by using battery energy storage (BES) along with PV array [2].

There are several configurations, which are available for integrating the PV array and BES into the utility grid. A single stage grid interfaced solar PV-BES system is reported in the literature with maximum power extracting capability [3].A grid integrated PV-BES system involving two stage conversion is also reported in the literature [4], where the extraction of maximum power from the PV array is achieved by using maximum power point tracking (MPPT) control, which generates duty cycle for the dc–dc converter. This article presents PV-BES-based microgrid system with the main features of maximum power extraction from the PV array, balancing of grid currents, unity power factor (UPF) operation at grid side, harmonics elimination, SA mode of operation and seamless transition from the GC mode to SA mode and vice versa.

In existing method instantaneous reactive power theory, synchronous reference frame theory, instantaneous symmetrical component theory, Least Mean Square (LMS), hyperbolic tangent function, digital disturbance estimator are used for power quality improvement. In proposed system Leaky Least Mean Mixed Norm (LLMMN) adaptive control is used for controlling the VSC in the Grid Connected (GC) mode of operation.

A leakage-based variant of the Least Mean Mixed Norm (LMMN) algorithm and the leaky Least Mean Mixed Norm (LLMMN) [15] algorithm will help mitigate the weight drift problem experienced in the conventional Least Mean Square (LMS) and Least Mean Fourth (LMF) algorithms. In the case of LMMN, the parameter drift causes the adaptive filter weights to blow up while in the case of the leaky LMMN, the adaptive filter weights are bounded.

II. SYSTEM CONFIGURATION

The PV-BES based microgrid [20] is depicted in Fig. 1. It includes a PV array a BES, a BDDC, a three-leg VSC, three-phase grid, and nonlinear loads. The grid outage and grid restoration, are realized by using a solid-state switch at the grid side. Ripple filters are used at the grid side and the load side, to remove the ripples in voltages. ABDDC is used for controlling the charging and discharging of the BES. A DSP (d-SPACE 1006 real-time controller) is used for generating the switching signals to the VSC.
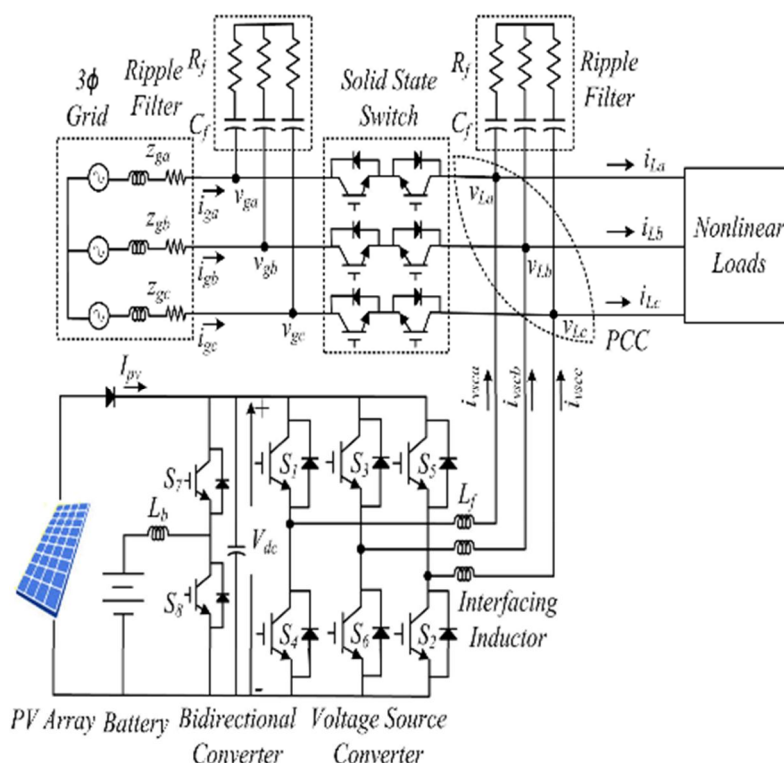
Fig.1 Multifunctional PV-BES microgrid configuration

This system is operating in two modes. One is in GC mode when the grid is present and the other is in SA mode when the grid is absent. The structure of VSC control is depicted in Fig. 2. In GC mode, if BES is present, then VSC is operated to feed a constant power to the grid. Here, BDDC maintains the dc-link voltage to the desired voltage. If BES is absent in the system, then the VSC performs the regulation of the dc-link voltage to the desired voltage and this mode leads to variable power feeding to or drawing from the grid depending upon the PV generation and the load demand.
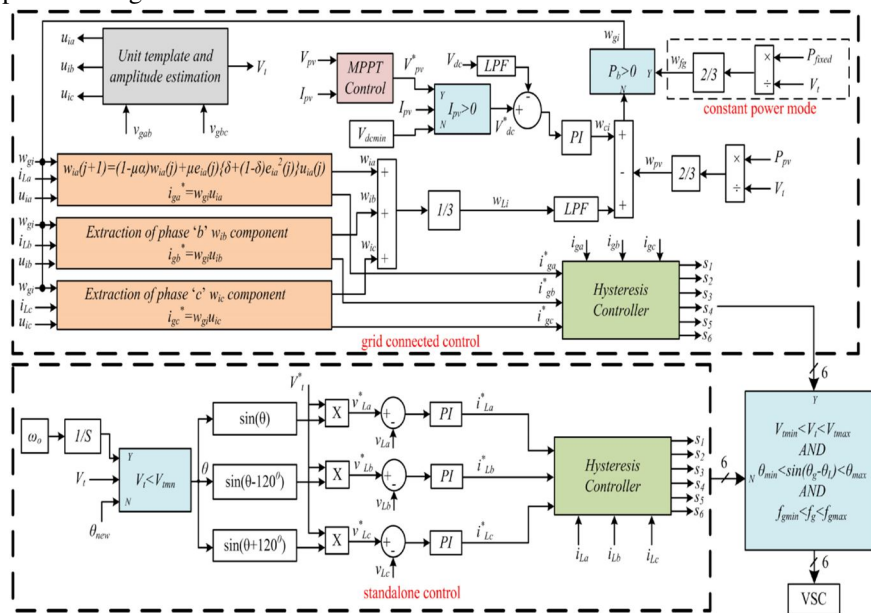

Fig.2 The control of VSC in GC mode of Operation

III.SIMULATION RESULTS

The simulated performance of the microgrid is studied using MATLAB/Simulink toolbox. The performance is studied under various operating conditions at a line voltage of 230 V, 50 Hz. The steady-state performance of the microgrid in the GC mode of operation is shown in Fig. 3.
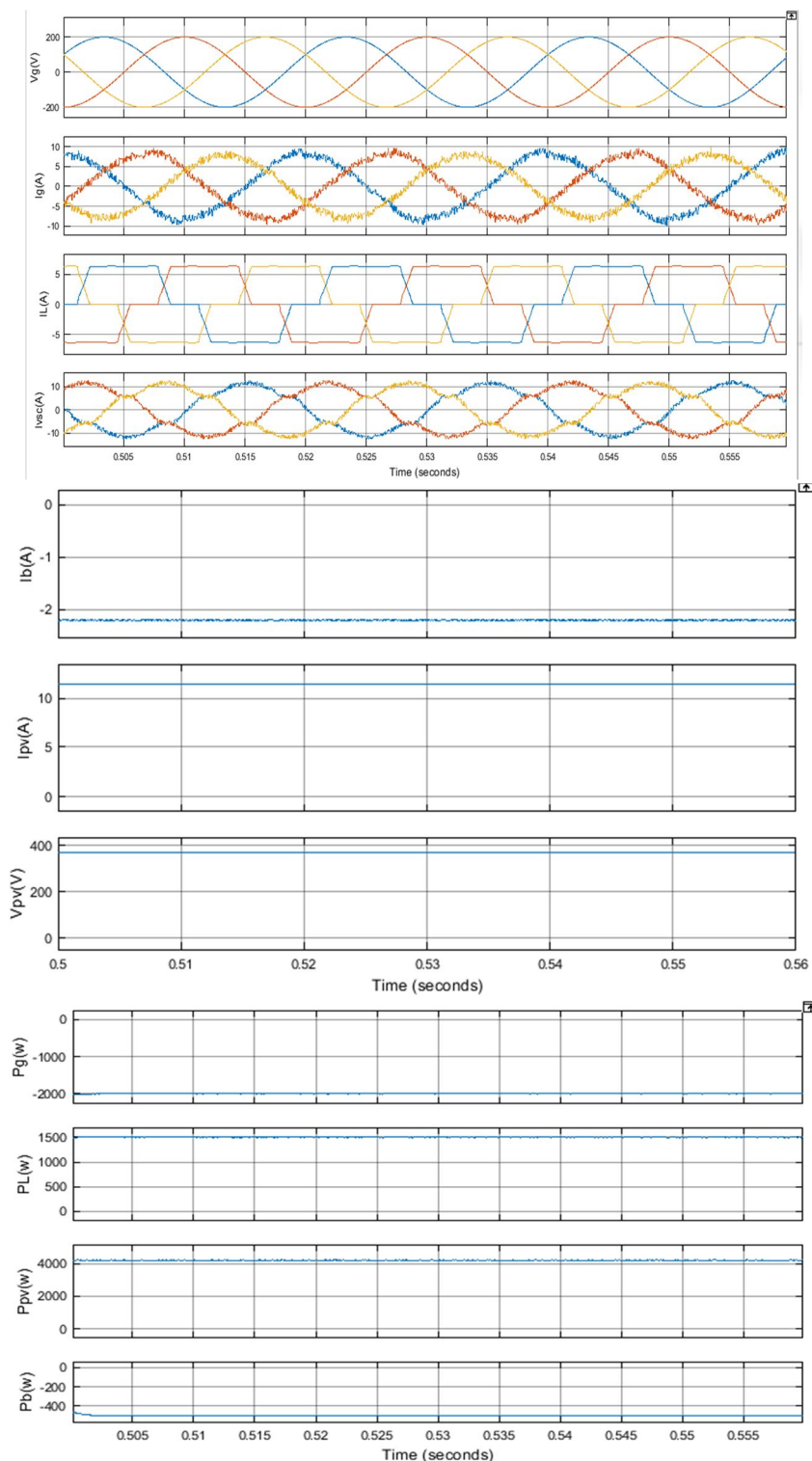

Fig. 3 Steady-state operation of the microgrid in GC mode

It shows grid voltages, grid currents, load currents, VSC currents, battery current, PV array current and voltage, grid power, load power, PV array output power, and battery power. It shows that the VSC injects the distorted currents such that the grid currents are maintained to sinusoidal. The grid currents are 1800 out of phase with the grid voltages since constant power is fed to the grid. The power output from the PV array at 1000 W/m2 solar radiation is 4.1 kW. The performance is studied by feeding a fixed power of 2 kW to the grid. The power output from the PV array is used to meet the load demand of 1.5 kW and to feed the fixed grid power. The remaining power is stored in the battery.

The steady-state performance of the microgrid in SA mode is shown in Fig. 4. It shows load voltages, load currents, battery current, PV array current and voltage, PV array output power, load power, and battery power.
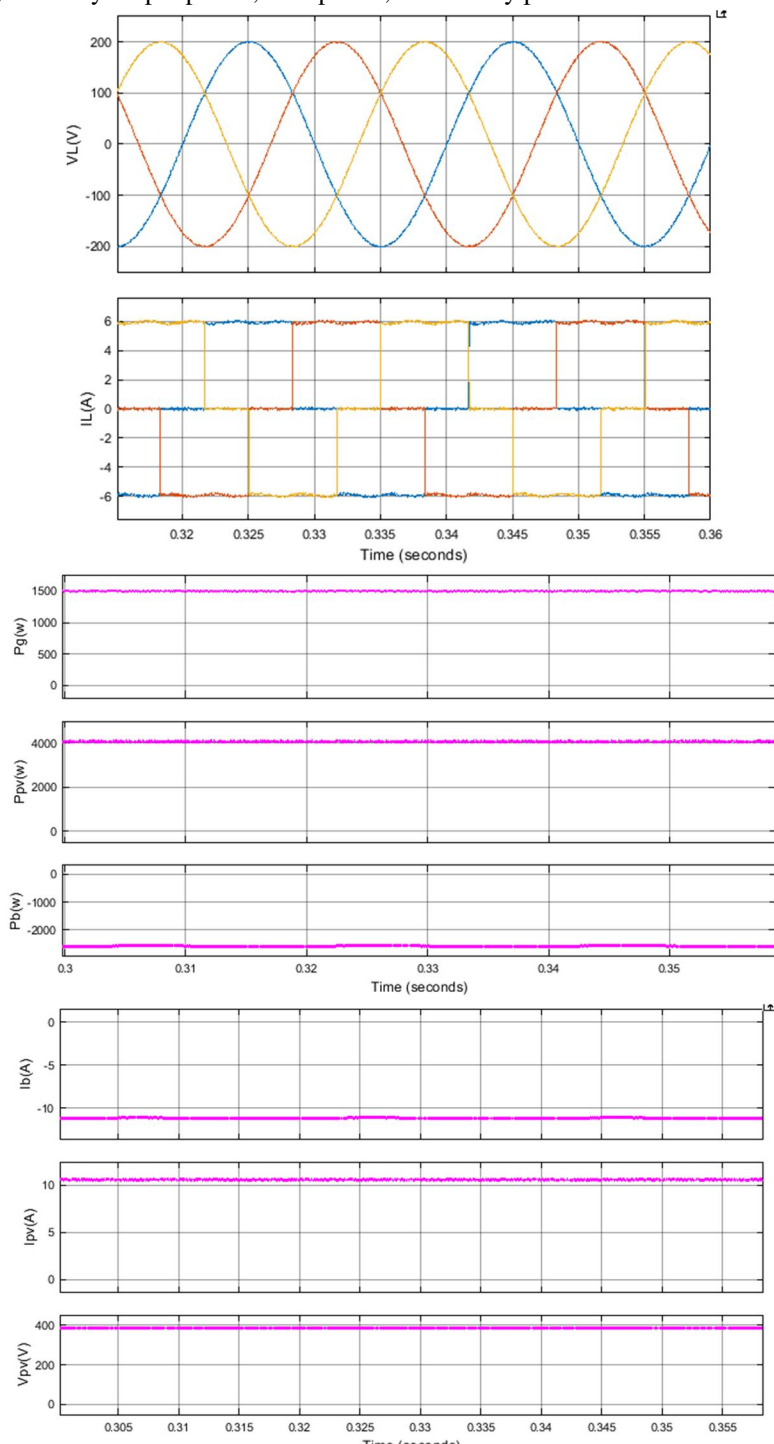

Fig. 4 Steady-state operation of the microgrid in SA mode

Sinusoidal, balanced, and distortion free voltages are generated with desired frequency by a proper SA control algorithm. The dc-link voltage is regulated to the desired voltage by controlling the BDDC. The performance is studied at 1000 W/m2 solar irradiation. The power output of the PV array at this irradiation is 4.1 kW. The power demanded by the load is 1.5 kW. The PV array meets the load demand and the remaining power is stored in the battery.

The performance of the micro grid at varying solar irradiation is shown in Fig. 5. It shows grid voltages, grid currents, load currents, VSC currents, battery current, PV array current and voltage, grid power, load power, PV array power, and battery power.
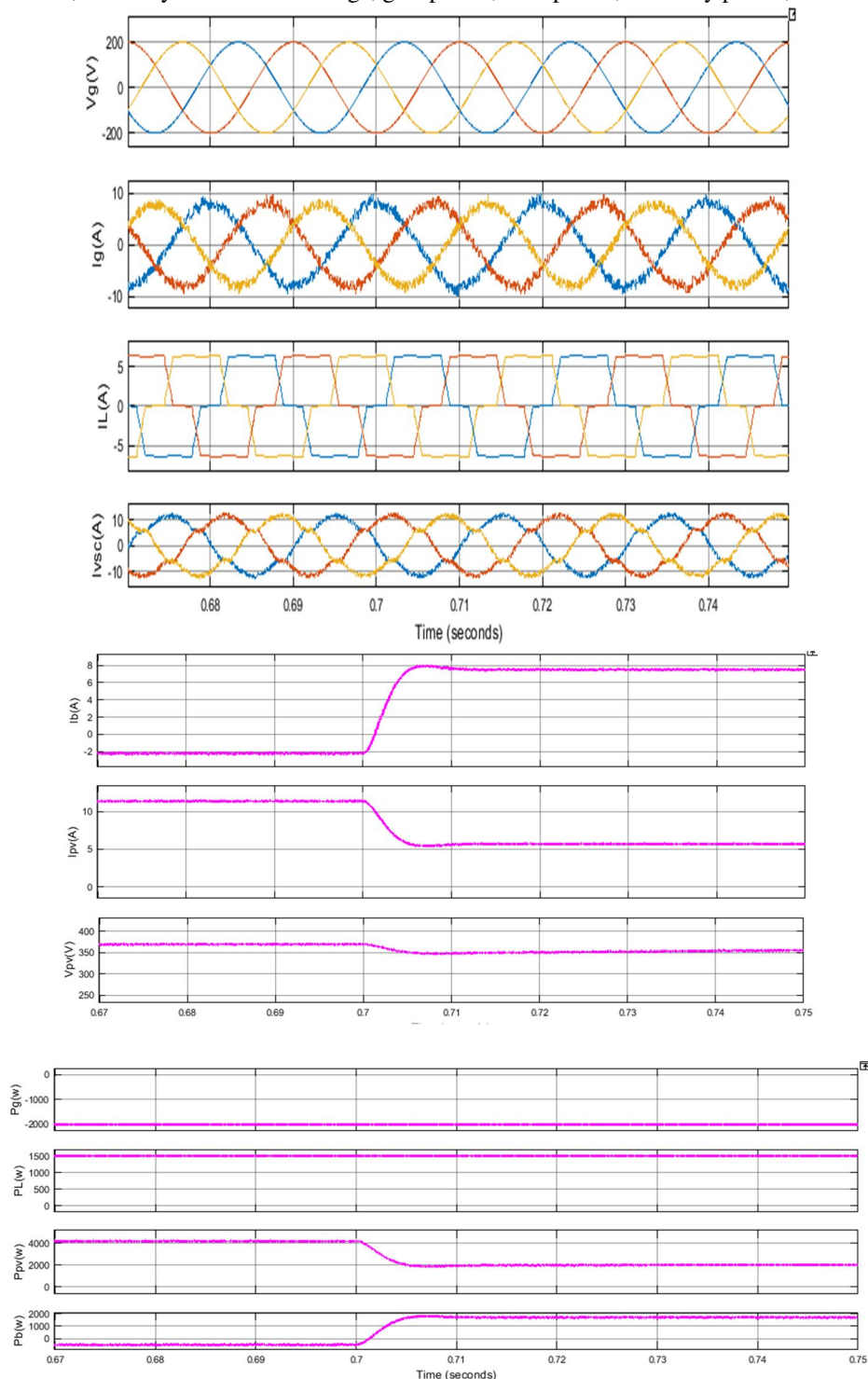

Fig. 5 Performance of microgrid under a change in the level of solar irradiation.

The performance is studied by reducing the solar irradiation from 1000 to 500 W/m2. Since the performance is studied by feeding a fixed amount of power to the grid hence the variation in the PV array output power is not reflected at the grid. A fixed power of 2 kW is fed to the grid and the power demand of connected load is 1.5 kW. Initially, at 1000W/m2 solar irradiation, the power output from the PV array is 4.1 kW. So the PV array meets the load demand and the fixed grid power and the remaining power is stored in the battery. Hence, the battery is operated in the charging mode. At 0.7 s, the solar irradiation is reduced to 500 W/m2, hence its power output is reduced to 2.05 kW. Since the power output from the PV array is insufficient to meet the load demand and the fixed grid power hence the battery delivers remaining power. Hence, the battery is operated in the discharging mode at 500 W/m2 solar irradiation.

The seamless transfer capability of the microgrid from GC mode to SA mode is shown in Fig. 6. It shows the grid voltage and load voltage of three phases, grid currents, load currents, VSC currents, phase angles of grid and load voltages, PV array voltage and current, and the battery current.
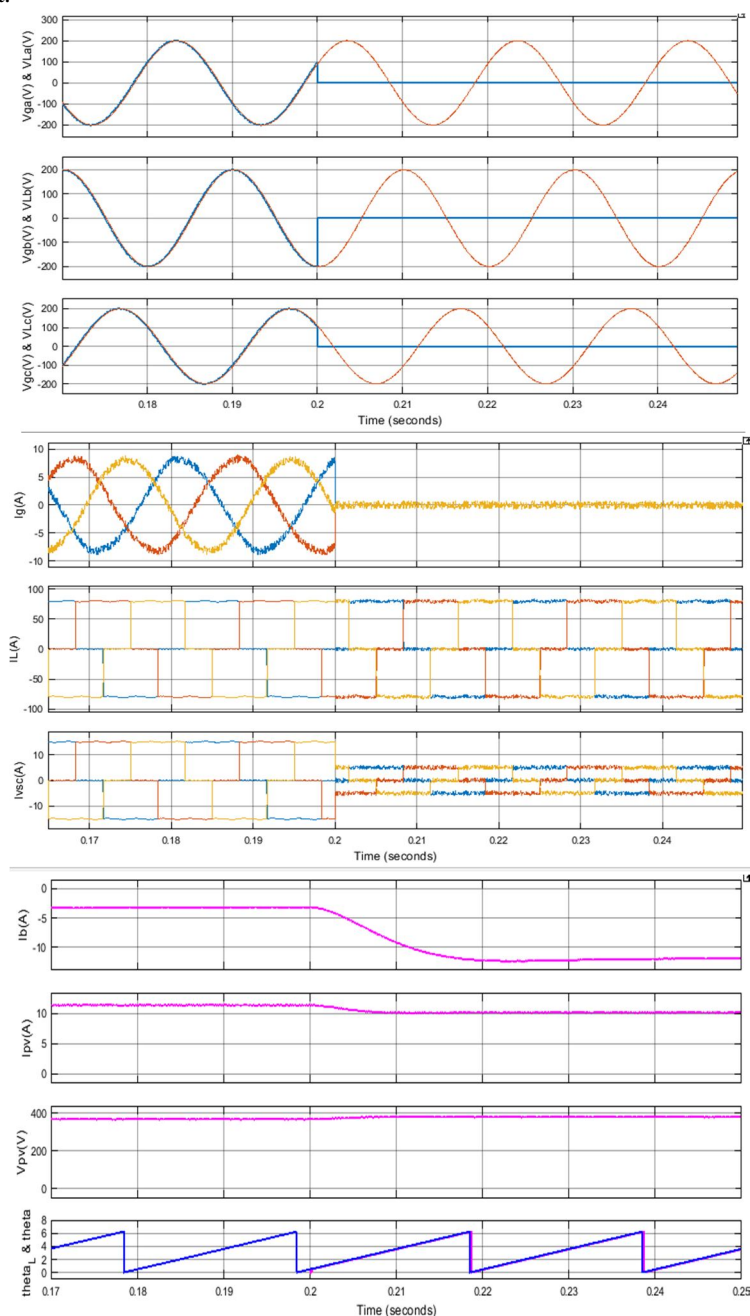

Fig. 6 Seamless transition of microgrid from GC mode to SA mode.

The seamless transfer capability of the microgrid from SA mode to GC mode is shown in Fig. 7. It shows grid voltage and load voltage of three phases, grid currents, load currents, VSC currents, phase angles of grid and load voltages, PV array voltage and current, and the battery current. Initially, the microgrid is operated in SA mode. At 0.4 s, the main grid is recovered. However, the main grid is connected to the microgrid only whenever the voltage magnitude, frequency, and phase angles have become in the desired set limits. Initiallythe phase angles of the load voltages and the grid voltages are mismatched.
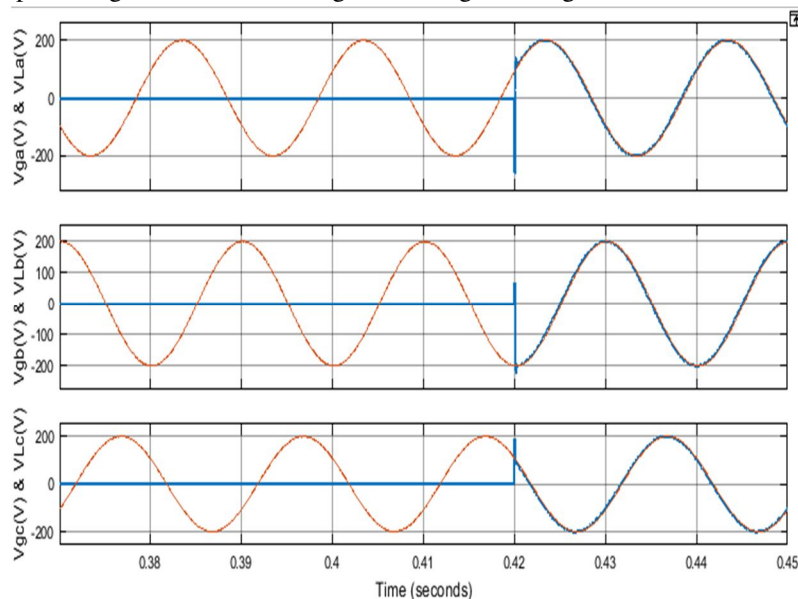
The phase angles of the grid voltages and the load voltages are matched at 0.42 s. Thereby the fixed amount of currents flows to the grid only at 0.42 s. Initially, the microgrid is operated in SA mode and the PV array meets the load demand and excess power available is stored in the battery. After the reconnection of the main grid into the microgrid, the PV array meets load demand and fixed grid power and remaining power is stored in the battery. Hence, the battery charging current is reduced in the GC mode of the microgrid.
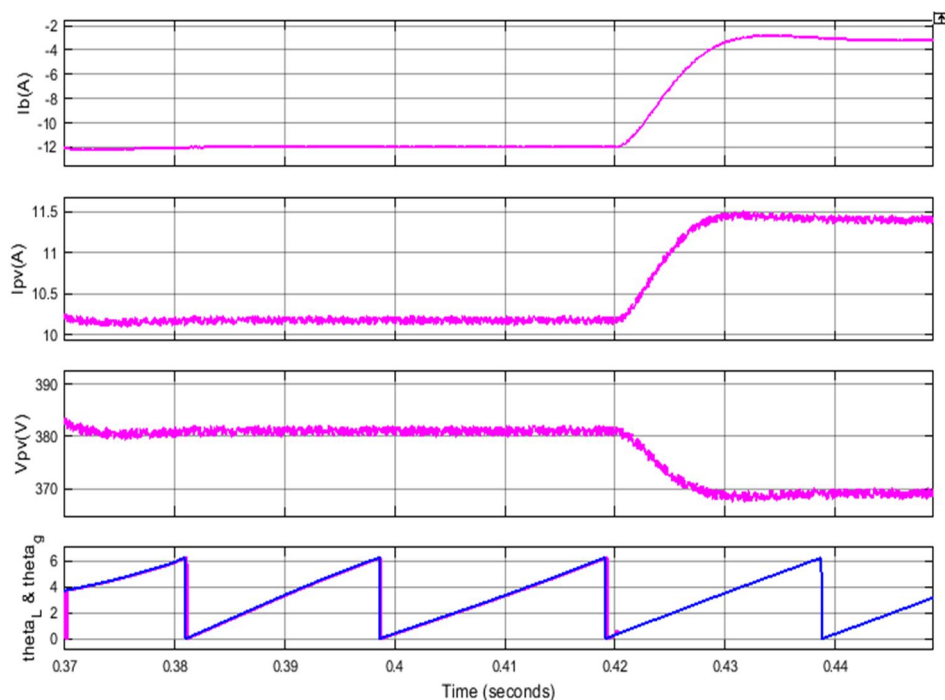

Fig. 7 Seamless transition of microgrid from SA mode to GC mode.

Simulation Parameters	PV array	$N_s = 21$, $N_p = 1$, $V_{mpp} = 373V$, $I_{mpp} = 10.8A$, $P_{mpp} = 4.1kW$
	DC link capacitor	$C_{dc} = 3mF$
	Battery	240V, 49Ah
	Grid voltage	$V_{LL} = 230V$ (rms), 50Hz
	Interfacing inductor	$L_f = 4mH$
	Switching frequency	$f_s = 10kHz$
	Control parameters	$\mu = 0.0156$, $\delta = 0.5$, $\alpha = 0.12$
	Synchronization limits	$V_{tmin} = 180V$, $V_{tmax} = 195V$, $V_{tmn} = 170V$, $f_{gmin} = 49.5Hz$, $f_{gmax} = 50.5Hz$, $\theta_{min} = -0.01$, $\theta_{max} = 0.01$
Experimental Parameters	PV array	$V_{mpp} = 363V$, $I_{mpp} = 11.7A$, $P_{mpp} = 4.25kW$
	DC link capacitor	$C_{dc} = 3mF$
	Battery	240 V, 49Ah
	Grid voltage	$V_{LL} = 230V$ (rms), 50Hz
	Interfacing inductor	$L_f = 4mH$
	Switching frequency	$f_s = 10kHz$
	Control parameters	$\mu = 0.0156$, $\delta = 0.5$, $\alpha = 0.12$
	Synchronization limits	$V_{tmin} = 180V$, $V_{tmax} = 195V$, $V_{tmn} = 170V$, $f_{gmin} = 49.5Hz$, $f_{gmax} = 50.5Hz$, $\theta_{min} = -0.01$, $\theta_{max} = 0.01$

The comparative analysis depicts that the proposed LLMMN control gives better performance than the conventional LMMN and LMS controls as shown in figure 8. It shows that the oscillation in weight with the LLMMN control is much lesser than the conventional least mean mixed norm and LMS control algorithms.
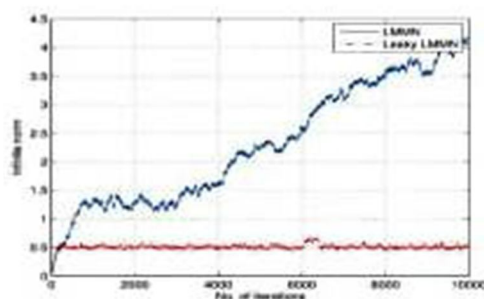

Fig. 1. Comparison of the LMMN and leaky LMMN in a weight drift environment

Fig. 8 Comparison of the LMMN AND leaky LMMN in the weight drift environment

IV. CONCLUSIONS

The operation of the microgrid in different modes is investigated in this work, which proves the multifunctional capability of the system. It is observed that system operates in both GC mode and SA mode without causing any interruptions in load supply and also performed the seamless transition capability from GC mode to SA mode and vice versa. A BDDC performs the extraction of maximum power from the solar PV array when the BES is active in system performance. Whenever the BES becomes inactive, then the MPPT control is automatically shifted to VSC control, thereby the PV array is operated at its MPP in all operating conditions. The comparative analysis depicts that the proposed LLMMN control gives better performance than the conventional LMMN and LMS controls. It shows that the oscillation in weight with the LLMMN control is much lesser than the conventional least mean mixed norm and LMS control algorithms.

REFERENCES

[1] E. Goutard, "Renewable energy resources in energy management systems," in Proc. IEEE PES Innovative Smart Grid Technol. Conf. Europe, 2010, pp. 1–6.
[2] P. Andea, A. V. Mnerie, F. Solomonesc, O. Pop, and D. Cristian, "Conventional vs. alternative energy sources overview. Part II. European strategies," in Proc. Int. Joint Conf. Comput. Cyber. Tech. Informat., 2010, pp. 601–606.
[3] B. S. Shatakshi and S. Mishra, "Dual mode operational control of single stage PV-battery based microgrid," in Proc. IEEMA Eng. Inf. Conf., 2018, pp. 1–5.
[4] N. Saxena, I. Hussain, B. Singh, and A. L. Vyas, "Solar PV interfaced to multifunctional VSC with a battery support," in Proc. IEEE Power India Int. Conf., 2016, pp. 1–6.
[5] B. Singh, A. Chandra, and K. Haddad, Power Quality: Problems and Mitigation Techniques. New Delhi, India: Wiley, Jan. 2015.
[6] B. Singh, P. Jayaprakash, D. P. Kothari, A. Chandra, and K. A. Haddad, "Comprehensive study of DSTATCOM configurations," IEEE Trans. Ind. Informat., vol. 10, no. 2, pp. 854–870, May 2014.

[7] M. Barghi Latran, A. Teke, and Y. Yolda¸s, "Mitigation of power quality problems using distribution static synchronous compensator: A comprehensive review," IET Power Electron., vol. 8, no. 7, pp. 1312–1328, Jul. 2015.

[8] N. D. Tuyen and G. Fujita, "PV-active power filter combination supplies power to nonlinear load and compensates utility current," IEEE Power Energy Technol. Syst. J., vol. 2, no. 1, pp. 32–42, Mar. 2015.

[9] V. Narayanan and P. Jayaprakash, "Performance comparison of threephase four-wire grid integrated solar photovoltaic system with various control algorithms," in Proc. Int. Conf. Intell. Comput., Instrum. Control Technol., 2017, pp. 406–414.

[10] M.V. ManojKumar, M. K. Mishra, and C.Kumar, "A grid-connected dual voltage source inverter with power quality improvement features," IEEE Trans. Sustain. Energy, vol. 6, no. 2, pp. 482–490, Apr. 2015.

[11] B. Singh and J. Solanki, "An implementation of an adaptive control algorithm for a three-phase shunt active filter," IEEE Trans. Ind. Electron., vol. 56, no. 8, pp. 2811–2820, Aug. 2009.

[12] Swain and B. Subudhi, "A new grid synchronisation scheme for a three-phase PV system using self-tuning filtering approach," IET Gener., Transmiss. Distrib., vol. 11, no. 14, pp. 3557–3567, Sep. 2017.

[13] V. Jain, I. Hussain, and B. Singh, "A HTF-based higher-order adaptive control of single-stage grid-interfaced PV system," IEEE Trans. Ind. Appl., vol. 55, no. 2, pp. 1873–1881, Mar./Apr. 2019.

[14] S. Pradhan, B. Singh, and B.K. Panigrahi, "Adigital disturbance estimator (DDE) for multi-objective grid connected solar PV based distributed generating system," IEEE Trans. Ind. Appl., vol. 54, no. 5, pp. 5318–5330, Sep./Oct. 2018.

[15] M. A. Nasar and A. Zerguine, "The leaky least mean mixed norm algorithm," in Proc. Asilomar Conf. Signals, Syst. Comput., 2013, pp. 1520–1523.

[16] M. N. Arafat, S. Palle, Y. Sozer, and I. Husain, "Transition control strategy between standalone and grid-connected operations of voltagesource inverters," IEEE Trans. Ind. Appl., vol. 48, no. 5, pp. 1516–1525, Sep./Oct. 2012.

[17] X. Li, H. Zhang, M. B. Shadmand, and R. S. Balog, "Model predictive control of a voltage-source inverter with seamless transition between islanded and grid-connected operations," IEEE Trans. Ind. Electron., vol. 64, no. 10, pp. 7906–7918, Oct. 2017.

[18] S. Kumar and B. Singh, "Seamless operation and control of single-phase hybrid PV-BES-utility synchronized system," IEEE Trans. Ind. Appl., vol. 55, no. 2, pp. 1072–1082, Mar./Apr. 2019.

[19] T. H. Nguyen, K. Al Hosani, N. Al Sayari, and A. R. Beig, "Seamless transition scheme between grid-tied and stand-alone modes of distributed generation inverters," in Proc. IEEE 3rd Int. Future Energy Electron. Conf. ECCE Asia, 2017, pp. 344–349.

[20] V. Narayanan, Seema, and B. Singh, "Solar PV - BES based microgrid system with multifunctional VSC," in Proc. 5th IEEE Sect. Int. Conf. Elect., Electron. Comput. Eng., 2018, pp. 1–6.

[21] J. Zhang and Q. Zhang. "Derivation and conformity measurement of a popular explicit analytic Borowy 2C PV modulemodel," J. Modern Power Syst. Clean Energy, vol. 2, no. 4, pp. 431–437, Dec. 2014.

[22] J. J. Nedumgatt, K. B. Jayakrishnan, S. Umashankar, D. Vijayakumar, and D. P. Kothari, "Perturb and observe MPPT algorithm for solar PV systems-modeling and simulation," in Proc. Annu. IEEE Ind. Conf., 2011, pp. 1–6.

[23] Z. Xuesong, S. Daichun, M. Youjie, and C. Deshu, "The simulation and design for MPPT of PV system based on incremental conductance method," in Proc. WASE Int. Conf. Inf. Eng., 2010, pp. 314–317.

[24] Shweta Sankhla, Dr. M. K. Bhaskar, Manish Parihar, " Analysis of an Anti-Islanding Prevention Technique in a Grid-Connected PV System", International Journal of Scientific Research in Science and Technology(IJSRST), Print ISSN : 2395-6011, Online ISSN : 2395-602X, Volume 10, Issue 4, pp.583-587, July-August-2023

[25] D. Baimel, R. Shkoury, L. Elbaz, S. Tapuchi, and N. Baimel, "Novel optimized method for maximum power point tracking in PV systems using fractional open circuit voltage technique," in Proc. Int. Symp. Power Electron., Elect. Drives, Autom. Motion, 2016, pp. 889–894.

[26] H. A. Sher, A. F. Murtaza, A. Noman, K. E. Addoweesh, K. Al-Haddad

[27] and M. Chiaberge, "A new sensorless hybrid MPPT algorithm based on fractional short-circuit current measurement and P&O MPPT," IEEE Trans. Sustain. Energy, vol. 6, no. 4, pp. 1426–1434, Oct. 2015.

[28] M. Rakhshan, N. Vafamand, M. Khooban, and F. Blaabjerg, "Maximum power point tracking control of photovoltaic systems: A polynomial fuzzy model-based approach," IEEE J. Emerg. Sel. Topics Power Electron., vol. 6, no. 1, pp. 292–299, Mar. 2018.

INTERNATIONAL JOURNAL FOR RESEARCH

IN APPLIED SCIENCE & ENGINEERING TECHNOLOGY

Call : 08813907089 ○ (24*7 Support on Whatsapp)